

Article

On the role of lattice oxygen in oxygen evolution reaction on CoO: isotope exchange determined using a new *small-volume* DEMS cell design

Hatem M.A. Amin, Heinz-Peter Königshoven, Martina Hegemann, and Helmut Baltruschat

Anal. Chem., **Just Accepted Manuscript** • DOI: 10.1021/acs.analchem.9b01749 • Publication Date (Web): 16 Sep 2019Downloaded from pubs.acs.org on September 17, 2019**Just Accepted**

"Just Accepted" manuscripts have been peer-reviewed and accepted for publication. They are posted online prior to technical editing, formatting for publication and author proofing. The American Chemical Society provides "Just Accepted" as a service to the research community to expedite the dissemination of scientific material as soon as possible after acceptance. "Just Accepted" manuscripts appear in full in PDF format accompanied by an HTML abstract. "Just Accepted" manuscripts have been fully peer reviewed, but should not be considered the official version of record. They are citable by the Digital Object Identifier (DOI®). "Just Accepted" is an optional service offered to authors. Therefore, the "Just Accepted" Web site may not include all articles that will be published in the journal. After a manuscript is technically edited and formatted, it will be removed from the "Just Accepted" Web site and published as an ASAP article. Note that technical editing may introduce minor changes to the manuscript text and/or graphics which could affect content, and all legal disclaimers and ethical guidelines that apply to the journal pertain. ACS cannot be held responsible for errors or consequences arising from the use of information contained in these "Just Accepted" manuscripts.

1
2 **On the role of lattice oxygen in oxygen evolution reaction on Co_3O_4 : isotope exchange**
3 **determined using a new *small-volume* DEMS cell design**
4
5
6
7
8
9
10
11

12 Hatem M.A. Amin^{a,b}, Peter Königshoven^b, Martina Hegemann^b, Helmut Baltruschat^{b,*}
13
14
15
16

17 ^a Department of Chemistry, Faculty of Science, Cairo University, 12613 Giza, Egypt
18

19 ^b Institute of Physical and Theoretical Chemistry, University of Bonn, 53117 Bonn, Germany
20
21
22
23

24 * Corresponding author: baltruschat@uni-bonn.de
25 hatem@pc.uni-bonn.de
26
27
28
29
30
31
32
33
34
35
36
37
38
39
40
41
42
43
44
45
46
47
48
49
50
51
52
53
54
55
56
57
58
59
60

Abstract

This work demonstrates the role of lattice oxygen of metal oxide catalysts in oxygen evolution reaction (OER) as evidenced by isotope labeling together with differential electrochemical mass spectrometry (DEMS) method. Our recent report assessed this role for Co_3O_4 using a flow-through DEMS cell, which however requires a large volume of electrolyte. Herein, we extend this procedure to different Co_3O_4 catalyst loadings and particle sizes as well as the mixed $\text{Ag}+\text{Co}_3\text{O}_4$ catalyst. We introduce, for the first time, a novel *small-volume* DEMS cell design capable of using disc electrodes and only < 0.5 mL of electrolyte. The reliability of the cell is demonstrated by monitoring gas evolution during OER in real time. This cell shows high sensitivity, high collection efficiency and very short delay time. DEMS results reveal that only the interfacial part ($\sim 0.2\%$ of the total loading or 25% of surface atoms) of the catalyst is active for OER. Interestingly, the amount of oxygen exchanged on the mixed $\text{Ag}+\text{Co}_3\text{O}_4$ catalyst is higher than that on the single Co_3O_4 catalyst, which illustrates the improved electrocatalytic activity previously reported on this mixed catalyst. Furthermore, the real surface area of the catalysts is estimated using different methods (namely ball model, double layer capacitance, isotope exchange and redox peak methods). The surface area estimated from BET and ball model are comparable, but roughly three times higher than that of the redox peak method. Our method represents an alternative approach for probing the mechanism and real surface area of catalysts.

Keywords: Water electrolysis; new DEMS cell; cobalt oxide; real surface area; isotope labeling

1. Introduction

The development of a cost-effective and highly active catalyst is of significant importance for energy storage applications such as metal-air batteries and fuel cells. Oxygen evolution reaction (OER), in particular, is a central process in these energy technologies. In the last few decades, the intensive research has resulted in the development of materials with diverse electrocatalytic and redox properties.^{1,2} However, OER kinetics is still sluggish and the commercially used catalysts are based on precious metals.³

First-row transition metal oxides in particular Co-based materials⁴⁻⁶ are inexpensive alternatives to the state-of-the-art IrO₂,^{7,8} and have significantly shown high activity for OER.^{9,10} Additionally, some bimetallic catalysts such as Ag+Co₃O₄ mixture^{4,11,12} have shown bifunctional oxygen activity.¹³

In addition to the great efforts that have been exerted to explore highly active catalysts, substantial effort has been directed to understand the mechanism of OER.^{9,14,15} As a result, several reaction mechanisms have been reported¹⁵⁻¹⁸ and it is highly complicated to assign a single reaction step to oxygen electrocatalysis on oxide surfaces. In most of the previously reported mechanisms, changes in the oxidation states of the metal take place during OER, and thus are mainly responsible for the enhanced activity observed at cobalt-containing catalysts.^{4,19,20} Bergmann et al. reported that only the outermost part of the Co-oxide (1.8% of Co ions) takes part in the redox reactions.²⁰ Switzer et al. demonstrated the conversion of Co(OH)₂ to CoOOH and Co₃O₄ and compared their OER activity. CoOOH and Co₃O₄ showed to have the same OER Tafel slope when the current is corrected for the electrochemically active surface area, suggesting the importance of assessing the real surface area and that the active species in both materials is likely to be Co^{IV}.²¹ Using X-ray photoelectron spectroscopy, we previously showed a reversible redox switching in Co₃O₄ when it is in contact with Ag in a mixture.⁴

A different mechanism, in which the lattice oxygen of the oxide catalyst is involved in oxygen evolution and formic acid oxidation, has been proven by mass spectrometry together with isotope labeling method.²²⁻²⁸ However, this OER mechanism may not be generalized to all metal oxides as it is dependent on the composition, structure and crystallinity of the material: Although most of the investigated catalysts including Co₃O₄,²² RuO₂,^{29,30} IrO₂,²⁴ Ba_{0.5}Sr_{0.5}Co_{0.8}Fe_{0.2}O_{3- δ} ³¹ and highly covalent perovskites³² showed lattice exchange, others including NiFeO_xH_y,²⁷ less covalent perovskites³² and oriented RuO₂ thin films¹⁸ do not. Using operando XAS, Schmidt and co-workers have recently demonstrated the involvement of lattice oxygen in OER.³¹ In our previous report²² we showed using differential electrochemical mass spectrometry (DEMS) technique that the lattice atoms of Co₃O₄ participate in OER via an oxygen exchange process. In this study, we extend our investigations to other Co₃O₄ catalyst loadings and particle sizes as well as to the mixed

1 Ag+Co₃O₄ catalyst, a catalyst of outstanding activity. This work thus correlates the activity with
2 the lattice oxygen exchange process in the oxide.
3

4
5 In the last two decades, different designs of DEMS cells have been developed to accommodate the
6 electrode's geometry and the purpose of the experiment.³³⁻³⁷ For example, in our previous report²²
7 on isotope labeling experiments, we used the thin-layer flow-cell which needs large amount of
8 electrolyte. The *classical* cell on the other hand has practical difficulty for employing solid
9 particles by drop cast and dry method.^{24,33} Therefore, the high cost of the isotope labeled water
10 consumed in the flow cell and the need for measurements with particle catalysts boosted us to
11 develop a new *small-volume* DEMS cell design, and is presented in this work for the first time (see
12 Fig. 1). In essence, this is a thin layer cell similar to that of *ref*^{36,38}, but the thin layer gap is
13 variable. In our design, important features are achieved: The use of small disc electrodes (5 mm)
14 and small electrolyte volume (≤ 0.5 mL) and particularly the very short delay time (≤ 2 s), which is
15 much less than that observed in other DEMS cells ($\sim 7-9$ s)^{27,30,35,39} and the recent sniffer-chip cell
16 (~ 3 s for OER).⁴⁰ The proof-of-concept of the new cell is examined for oxygen evolution by
17 probing the delay time, the ionic current signals and the characteristic features of voltammograms.
18
19 In practice, measuring the real surface area under the same conditions of the experiment is
20 important for catalyst assessment as the experimental conditions may change the state of electrode
21 surface. Here, we determine the true surface area using several approaches (namely, the ball
22 model, double-layer capacitance method, redox peak method and isotope exchange method). The
23 results of these methods are compared to the BET data. Thus, this work highlights the importance
24 of probing the mechanism and the surface area when assessing the catalyst activity.
25
26
27
28
29
30
31
32
33
34
35
36
37

38 **2. Experimental**

39
40 The chemicals, electrode preparation and experimental details can be found in the supporting
41 information.
42
43

44 *New small-volume DEMS cell*

45
46 A schematic drawing and an actual photo of the *small-volume DEMS cell* are shown in Fig. 1. A
47 common feature in most of DEMS cells is the use of a porous Teflon membrane interface which
48 achieves a shorter delay time^{33,37} compared to other DEMS setups with a gas carrier.^{34,40} In our
49 new design, a porous Teflon membrane interface is used.
50
51

52
53 For this cell, the working electrode is a GC bulk disc that allows the catalyst ink (e.g. Co₃O₄
54 powder in ethylene glycol) to be easily drop casted and dried onto it (In contrast, this is practically
55 difficult for cells that use a soft and shrinkable porous Teflon membrane as direct support for the
56 working electrode. Flow-through cells, which also can accommodate such an electrode, have the
57 disadvantage that the particle catalyst layer may not be stable enough under convective conditions
58
59
60

in addition to the higher electrolyte consumption). The disc electrode is then carefully installed and pressed into a Kel-F shaft so that both disc and shaft forefronts lie on the same planar level. The disc has a diameter of 5 mm (0.196 cm²). The shaft is an analogue to a RDE tip. It has a conical shape at the apex, as shown in the drawing, which results in good electrochemical performance. This shape is found to be important, after some trials with a pure cylindrical tip, as it allows a shorter distance between the disc and the reference electrode (ca. 3 mm). The tip containing the working electrode disc is inserted into a PTFE lid, and screwed into an upper Teflon mounting nut. The nut acts as a manipulator to control the distance of the working electrode from the Teflon membrane (range is from ~20 μm to ~3 mm). The Teflon lid tightly fits into the glass housing, which is made for a small-volume electrolyte. The glass cell is mounted on a stainless steel holder, which contains 5 mm diameter steel frit in the centre and is directly connected to a differentially pumped quadruple mass spectrometer MS (QMG-422, Pfeiffer). As an interface between the electrolyte and MS, a Teflon membrane is mechanically supported on the steel frit.

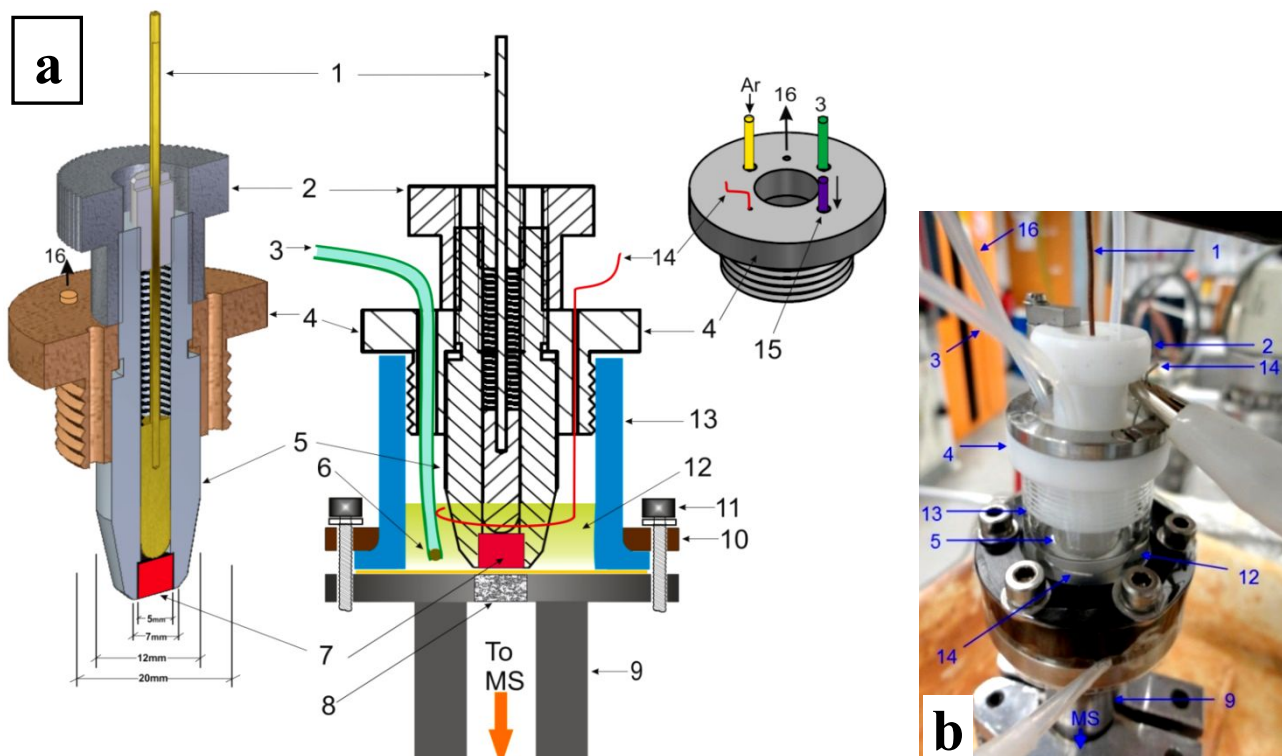


Fig. 1. a) Sketch and cross section of the new *small-volume DEMS cell* with its components, where 1) copper contact pin, 2) Teflon mounting nut, 3) reference electrode connection, 4) Teflon lid, 5) Kel-F shaft, 6) glass bead, 7) disc working electrode, 8) steel frit, 9) stainless steel connection to MS, 10) mounting ring, 11) steel screw, 12) electrolyte, 13) glass housing, 14) counter electrode, 15) electrolyte inlet and outlet, 16) gas outlet. b) Actual photo of the cell.

The working electrode was exactly facing the steel frit to allow efficient transfer of volatile products to MS. The working electrode was connected from the back side via a copper wire and a contact pin to get electrical contact with the potentiostat. Few tens of micrometers (~50 μm) is found to be the optimal distance between the working electrode and the membrane for our setup.

1
2 A Pt wire, as a counter electrode, was inserted through the PTFE lid to the electrolyte. The
3 reference electrode was a reversible hydrogen electrode (RHE). The reference electrode was
4 electrically connected to the working solution via a salt bridge made of a Teflon tube filled with
5 the same alkaline solution, and ended with a glass bead. All potentials in this work are referred to
6 RHE. Ar-purging was achieved by a Teflon tube, which was immersed into the solution at certain
7 distance from the membrane. The electrolyte was saturated with Ar for about 10 minutes prior to
8 and during the experiment. All experiments were carried out at room temperature (25 ± 1 °C).

14 3. Results

16 3.1. Oxygen exchange in Co_3O_4 (50 nm) catalyst in 20% marked H_2^{18}O solution

19 DEMS is a versatile technique that monitors the gaseous reaction products and intermediates of an
20 electrochemical reaction spectrometrically. To test the reliability of the new DEMS cell, OER at
21 $\text{Co}_3\text{O}_4/\text{GC}$ was monitored. In this experiment, Fig. 2, we used a higher catalyst loading ($400 \mu\text{g}$
22 cm^{-2}) and isotope concentration (20%) compared to our previous measurements with the flow thin
23 layer cell.²² In fact, the catalyst loading has an effect on the OER currents, where higher loadings
24 led to higher OER currents, see Fig. S1. In a similar procedure to that in our recently published
25 article,²² two series of experiments were conducted in the new cell: In *series A*, we performed the
26 experiments in marked H_2^{18}O solution to label the oxygen atoms of the Co_3O_4 with ^{18}O atoms;
27 while in *series B* the pre-labeled oxide was treated in unlabeled H_2^{16}O solution to evolve O_2 . By
28 monitoring the signals of different isotopic O_2 ($^{16}\text{O}_2$, $^{16}\text{O}^{18}\text{O}$ and $^{18}\text{O}_2$) we get information on the
29 extent of oxygen exchange in the oxide. From these experiments we prove that the oxygen of the
30 Co_3O_4 catalyst is involved in the OER mechanism. In *series A* of experiments, the cell was filled
31 from the electrolyte reservoir using a Teflon tube inlet with the marked solution: 0.8 M LiOH
32 solution containing 20% (w/w) of marked H_2^{18}O . CVs and MSCVs were recorded between 0.05 V
33 and 1.6 V vs. RHE for 6 cycles at a scan rate of 10 mV s^{-1} . Afterwards, the potential was stopped
34 at 0.4 V for electrolyte exchange for preparing for *series B*. Fig. 2a shows the respective
35 voltammograms for the first 3 cycles. The ionic currents corresponding to $^{16}\text{O}_2$, $^{16}\text{O}^{18}\text{O}$ and $^{18}\text{O}_2$
36 gases are clearly observable at potentials of OER (above 1.5 V), proving the successful operation
37 of the cell. In MSCV, the ionic currents correspond to the pure OER process, while in CV the
38 faradaic currents involve oxidation of Co_3O_4 at onset potentials of OER. Importantly, there is no
39 significant hysteresis between anodic and cathodic scans in the MSCV, as compared to the thin
40 layer cell³³ or the Kel-F cell used by Krtil et al.³⁰ The delay time in this cell is 1-2 s, as can be
41 noticed from the CVs and MSCVs. This proves the efficient mass transport to the mass
42 spectrometer in this cell.

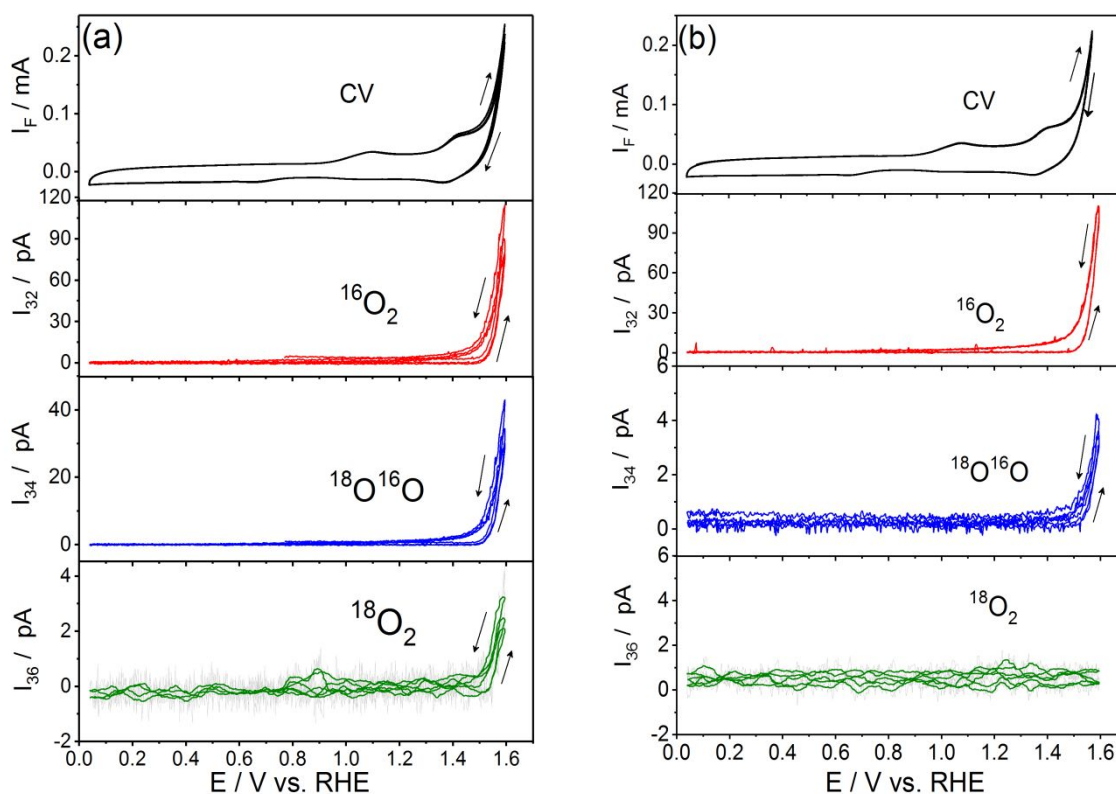


Fig. 2. CVs and MSCVs for OER (first 3 cycles) obtained at Co_3O_4 ($400 \mu\text{g}/\text{cm}^2$ of 50 nm size)/GC electrode in the new small-volume DEMS cell in (a) Ar-saturated 0.8M LiOH solution-containing 20% (w/w) marked H_2^{18}O , and the upper potential limit is 1.6 V, (b) 0.8M LiOH/ H_2^{16}O after the electrode has been pre-treated in 0.8M LiOH/ H_2^{18}O . The upper panel displays the faradaic current, while the lower ones represent the ionic currents for m/z 32, 34 and 36. Scan rate = 10 mV/s.

In addition to the validation of the quality of the cell, we aimed to investigate the contribution of the oxide in OER and its mechanism. After evaluation of the signals, the mole fraction of $^{16}\text{O}_2$ and $^{16}\text{O}^{18}\text{O}$ was calculated and displayed in Fig. 3a. The results show an increase of $^{16}\text{O}^{18}\text{O}$ concentration with a concomitant decrease in concentration of $^{16}\text{O}_2$ with each cycle, reaching steady-state values at the 4th cycle, see Fig. 3a. This indicates that the oxide indeed participates to some extent in OER. The assumption that the increase of $^{16}\text{O}^{18}\text{O}$ content in the evolved O_2 could be due to the exchange of an ^{16}OH by ^{18}OH can be ruled out since such OH groups would more probably exchanged during electrolyte exchange. Thus, they would not show up during OER. The plotted points in the figure represent the average of three data points due to the uncertainty in the integration of the peaks.

In *series B*, the marked solution was withdrawn from the cell using a syringe under constant potential of 0.4 V. The electrolyte was then replaced gradually while keeping a little of solution over the membrane; this process was repeated several times to ascertain the substitution of all the marked solution with H_2^{16}O solution. The pre-labeled oxide was then scanned in the fresh 0.8M LiOH/ H_2^{16}O solution for 7 cycles. Fig. 2b shows the first three cycles. The signal for $^{18}\text{O}_2$ is not

observable since its concentration is below limit of detection. The amount of $^{16}\text{O}^{18}\text{O}$ decreases with cycling reaching the final concentration of ^{18}O in solution, while the amount of $^{16}\text{O}_2$ increases, see Fig. 3b. This directly proves the oxygen exchange mechanism and participation of oxide atoms in OER. The steady-state values were reached after the 4th cycle, and the isotope content at/in the oxide is similar to that in the solution, thus no further exchange takes place. The isotopic composition of the formed O_2 correspond to a concentration of ~ 16.5 w% of H_2^{16}O . The difference from the as-prepared solution (20 w%) can be due to some losses on the walls of the syringe during transfer and thus dilution of the marked solution by the rest of water on the walls and membrane of the cell before start of measurement.

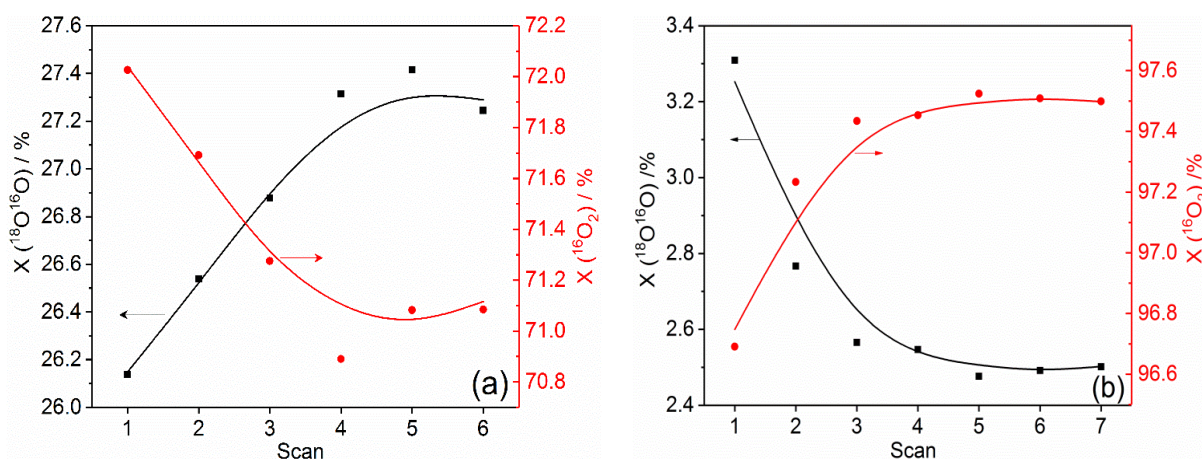


Fig. 3. Plot of the isotopic content as a function of scan number for OER obtained at Co_3O_4 ($400 \mu\text{g}/\text{cm}^2$)/GC with scan rate of $10 \text{ mV}/\text{s}$ in (a) $0.8\text{M LiOH}/(20 \text{ w}\%) \text{H}_2^{18}\text{O}$, (b) $0.8\text{M LiOH}/\text{H}_2^{16}\text{O}$, the electrode has been pre-treated in $0.8\text{M LiOH}/\text{H}_2^{18}\text{O}$. Data were taken from the experiment shown in Fig. 2. The uncertainty in X_{34} is $\sim 2\%$ and in X_{32} is $\sim 0.3\%$. The plotted data points represent the average of three independent integrations.

To determine quantitatively the extent of oxygen exchange process, the number of moles of exchanged oxygen atoms of the oxide were calculated and compared to the total atoms and also surface atoms of the catalyst, following the same procedure and equations reported in our previous study.²² For this catalyst loading, a total of $13.5 \text{ nmol cm}^{-2}$ oxygen atoms are exchanged, thus the amount of oxygen exchanged of the total oxygen atoms in Co_3O_4 loading is $r_{ex} \sim 0.2\%$. When the amount of exchanged oxygen is compared to the surface atoms obtained from the charge of the redox reaction $\text{Co}^{3+}/\text{Co}^{4+}$, we get the amount of exchanged atoms to the surface atoms $y_{ex} \sim 25\%$ which are active and participate in the oxygen exchange process, see Table 1. For comparison, previous results on IrO_2/Ti showed an isotope exchange of about 1-2% (few monolayers) of the total loading of the oxide.^{24,27}

Moreover, the real surface area of the catalyst is determined using different approaches: *i*) The *ball model* in which the particles were treated as spheres with homogenous radius, *ii*) *Double-layer DL capacitance* approach in which a DL capacitance of the oxide of $60 \mu\text{F cm}^{-2}$ is considered^{9,41}

although this value has a high degree of uncertainty. However, there are no well-accepted values for the DL capacitance for oxides including Co_3O_4 as they exhibit significant pseudo capacitance. *iii) Redox peak* method in which the moles of the surface atoms is calculated using the charge of the redox couple $\text{Co}^{3+}/\text{Co}^{4+}$ (peak at about 1.45 V), *iv) Isotope exchange* method based on the number of moles of atoms exchanged and *v) BET* analysis. Details of the procedure and the equations used for each method are described in our previous report.²² The results are summarized in Table 2 and compared in the discussion section.

Oxygen exchange in Co_3O_4 (50 nm) in 50% marked H_2^{18}O solution

We also studied the behavior of the same catalyst but in a higher H_2^{18}O concentration (50 w%) in solution and using higher upper potential limit (1.65 V), Fig. S2-S4. The results are displayed in Table 1 and revealed that the dependence of the isotope exchange ratio on the potential limit of scanning and the loading amount is not significant, see SI.

Table 1. Summary of results of oxygen exchange experiments at different catalysts and loadings.

Catalyst	$n_t(\text{O}^{2-}) / \text{nmol cm}^{-2}$	$r_{\text{surf}} / \%$	$r_{\text{ex}} / \%$	$y_{\text{ex}} / \%$	$r_{\text{ex}} / \%^{\#}$	$y_{\text{ex}} / \%^{\#}$
Co_3O_4 (40 μm) 100 $\mu\text{g}/\text{cm}^2$ in 0.5 M KOH with 2% isotope till 1.62 V ²²	1660	0.23	0.08	34	0.03	13
Co_3O_4 (50 nm) 200 $\mu\text{g}/\text{cm}^2$ in 0.1 M LiOH with 10% isotope till 1.8 V ²²	3320	1.78	0.22	12	0.1	8.5
Co_3O_4 (50 nm) 400 $\mu\text{g}/\text{cm}^2$ in 0.8 M LiOH with 20% isotope till 1.6 V	6640	0.79	0.20	25	0.05	6.4
Co_3O_4 (50 nm) 400 $\mu\text{g}/\text{cm}^2$ in 0.5 M LiOH with 50% isotope till 1.65 V(1.6 V)	6640	0.63	0.15(0.2)	23(22)	0.07(0.1)	11(3)
Co_3O_4 (10 μm) 600 $\mu\text{g}/\text{cm}^2$ in 0.8 M LiOH with 20% isotope till 1.61 V	9960	--	0.03	--	0.02	--
Ag+ Co_3O_4 (50 nm) 10 w%, 400 $\mu\text{g}/\text{cm}^2$ in 0.5 M LiOH with 50% isotope till 1.65 V	664	--	0.9	--	0.3	--
Ag+ Co_3O_4 (50 nm) 10 w%, 600 $\mu\text{g}/\text{cm}^2$ in 0.8M LiOH with 20% isotope till 1.65 V	664	--	0.7	--	--	--

$r_{\text{surf}} = n_{\text{surf}} / n_t$ is the ratio of moles of surface atoms (from surface redox peak charge) to the total number of moles in catalyst loading. (Not applicable to the catalysts mixed with Ag, because the corresponding peak is not separable from that belonging to Ag)

r_{ex} : Exchanged oxygen atoms to the total oxygen atoms in the catalyst loading

y_{ex} : Exchanged oxygen atoms to the oxygen atoms on the surface obtained from redox peak

Isotope exchange in H_2^{18}O -free solution after Co_3O_4 labeling (i.e. in *series B*)

3.2. Oxygen exchange in Co_3O_4 (10 μm) in 20% marked H_2^{18}O solution

It is widely recognized that the particle size of the catalyst influences its activity.²⁸ Therefore, we investigated this effect using RRDE and isotope labeling measurements, see Fig. S5 and S6. The results (Tables 1 and 2) proved the isotope exchange mechanism also for the large particles. According to the ball model, this catalyst should have a surface area of only about one hundredth of that of the 50 nm catalyst layer. The BET data, however, show that the real surface area is much

larger due to the intrinsic roughness of these larger particles. The real surface area that is obtained from the isotope exchange method in Series A at the 10 μm catalyst is roughly half of that obtained at the 50 nm catalyst suggesting an even larger roughness effect than the BET data. Correspondingly, the percentage of active surface sites as determined from the isotope exchange is twice as large as for the 50 nm particles (24% vs. 12 %).

3.3. Oxygen exchange at Ag+ Co₃O₄ (10 w%) mixed catalyst in 50% marked H₂¹⁸O solution

Recent literature showed that the mixed Ag 311+ Co₃O₄ catalyst has a marked catalytic activity for OER and ORR in alkaline media.^{4,11,12} Ag 311 stands for Ag particles from Ferro GmbH (and not for a crystallographic orientation). The enhanced bifunctionality was attributed possibly to a redox switching in Co₃O₄ (i.e. transitions between Co₃O₄ and Co(OH)₂).⁴ We thus investigated OER on the mixed catalyst based on Ag 311 (1 μm) + Co₃O₄ (50 nm) 10 w% in 0.5M LiOH solution containing 50% (w/w) of marked H₂¹⁸O, as shown in Fig. 4a. The redox peaks observed in the CV are assigned to oxidation and reduction of Ag and cobalt and their oxides. Ag is oxidized to Ag^IO and then further oxidized to Ag^IAg^{III}O₂.¹¹

In *series A* of experiments on the mixed catalyst, an increase of ¹⁶O¹⁸O concentration with a concomitant decrease of ¹⁶O₂ concentration with consecutive scans is observable, Fig. S7a. While in *series B* of experiments, a decrease of concentration of ¹⁶O¹⁸O with a concomitant increase in ¹⁶O₂ concentration with each cycle is noticed, see Fig. S7b. This behavior is similar to that observed on pure Co₃O₄ catalyst. Again, this supports the contribution of the oxide, and also could be the Ag-oxide since it is oxidized at higher potentials, in the oxygen exchange process. The total amount of ¹⁸O atoms exchanged during the successive scans corresponds to ~1% of the total loading with respect to only Co₃O₄ mass since Ag is mostly inactive for OER. The surface redox peak of cobalt oxide in the mixture is not separable from that belonging to Ag, and thus calculation of the r_{surf} and y_{ex} values is not applicable for the mixed catalyst. In *series B*, 0.3% is obtained, which is less than that in *series A*. This might be due to ¹⁸O interdiffusion or loss upon rinsing.

The above results show that the amount of surface atoms in the mixed Ag+ Co₃O₄ catalyst taking part in the oxygen exchange mechanism is higher than that observed on Co₃O₄ catalyst (~1% for the mixed catalyst compared to 0.2% for the Co₃O₄ catalyst). Roughly 50% of the surface atoms are active (for isotope exchange) as compared to 12 % for the pure 50 nm Co₃O₄ catalyst. Therefore, the surface of the mixed catalyst is more active than that of Co₃O₄. This suggests that OER takes place at the interphase between Co₃O₄ and Ag particles is important for OER in the mixture, but also that a spillover of oxygen atoms seems to be involved. This is important for the interpretation of the improved catalytic activity observed on the mixed catalyst.⁴ Thus, the real surface areas obtained from BET, ball model and isotope exchange model revealed good

qualitative agreement, illustrating the suitability of the used methods for the characterization of our catalysts, as displayed in Table 2. However, the results based on the DL capacitance method deviate from the other methods which might be because part of the exposed surface is oxide and the rest is metallic Ag.

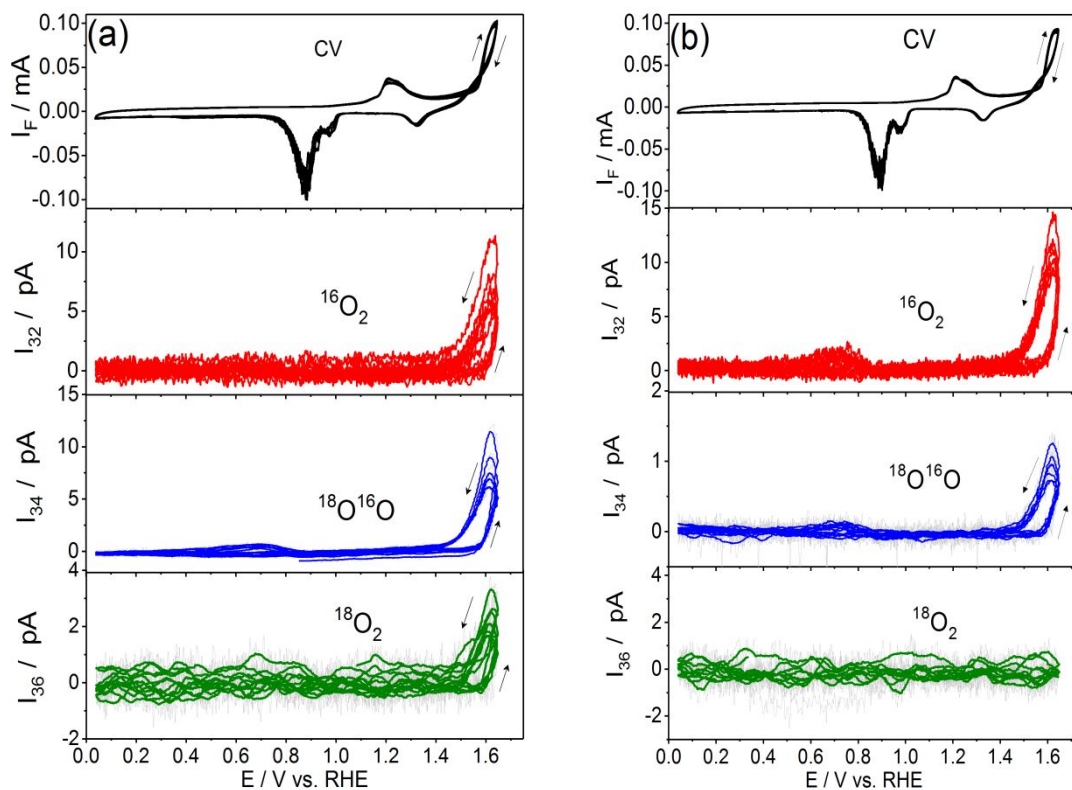


Fig. 4. DEMS results for 6 cycles OER at Ag + Co₃O₄ (10 w%) (400 μg/cm²)/GC electrode in the new small volume DEMS cell in (a) Ar-saturated 0.5M LiOH solution containing 50% (w/w) of marked H₂¹⁸O, scan rate=10 mV/s. (b) in 0.5M LiOH/H₂¹⁶O after the electrode has been pre-treated in 0.5M LiOH/H₂¹⁸O. The upper panel displays the faradaic current, while the lower ones represent the ionic currents for m/z 32, 34 and 36.

4. Discussion

A comparison of the results of different approaches to estimate the true surface area including the amount of exchanged oxygen (n) is given in Table 2. For the small particle size catalyst (50 nm), the ball model, redox peak model and the BET data revealed relatively good consistency, which indicates their smooth surface. However, for the larger particles (40 μm), the surface area estimated from the redox peak method is much larger than that obtained from the ball model, which seems to be due to their roughness. The results also show that the DL capacitance method gives higher true surface area than the BET method as the BET-determined surface area has not direct correlation to the electrochemically active area. Moreover, as can be noticed from the Table, the true surface area (roughness factor) obtained from the redox peak method for Co₃O₄ (50 nm) is roughly one-third to half of the BET value, indicating that only a part of the surface is active for surface redox reactions. Exception is the experiment in 0.1M LiOH in the thin layer cell, where the

1
2 ohmic resistance was too high so that the peaks are not well separated, thus the uncertainty in peak
3 charge could be high.²² In an independent experiment at Co_3O_4 (50 nm) with 1 mg cm^{-2} and 50 mV
4 s^{-1} in RRDE cell, the area calculated using the redox peak method is roughly one-third of the BET
5 value. This ratio is consistent with the results in our new cell.
6
7

8
9 Moreover, the true surface area obtained from isotope exchange method is a fraction (roughly a
10 quarter) of the surface area obtained from the redox peak method or corresponds roughly to 12 %
11 of the BET surface, suggesting that only a part of the surface atoms is exchanged. In particular
12 there is no indication of an exchange of subsurface oxygen atoms. No significant effect of catalyst
13 loading on the amount of exchanged oxygen of the total catalyst is observed. However, larger
14 surface area is obtained as the particle size decreases: the average true surface areas (obtained from
15 isotope exchange experiments) are 0.007 , 0.006 and $0.02 \text{ cm}^2_{\text{tr}}/\text{g}$ for the $40 \text{ }\mu\text{m}$, $10 \text{ }\mu\text{m}$ and 50 nm
16 Co_3O_4 catalysts, respectively. Additionally, the ‘active’ surface area (calculated from isotope
17 experiments) for the 50 nm catalyst increases as the loading of the catalyst increases from 200
18 $\mu\text{g}/\text{cm}^2$ to $400 \mu\text{g}/\text{cm}^2$, but the surface area obtained from DL capacitance and redox peak methods
19 does not increase accordingly, which could be due to the limited conductivity within the layer, see
20 Table 2. The fraction of oxygen atoms of the catalyst participating in oxygen exchange mechanism
21 approaches 0.2% of the total loading, independent of the loading. The true surface area of different
22 sizes of Co_3O_4 was in the order: $50 \text{ nm} > 10 \text{ }\mu\text{m} > 40 \text{ }\mu\text{m}$ which is reasonable, as depicted in Table 2.
23 Therefore, the transition from higher oxidation state oxide to lower oxidation state oxide, and thus
24 releasing oxygen, is possibly involved during OER at Co_3O_4 . This can be via an *oxygen exchange*
25 *mechanism*, in which surface lattice oxygen atoms of the oxide are exchanged with oxygen atoms
26 from the solution. A scheme correlating oxygen evolution reaction and the redox transitions in
27 Co_3O_4 catalyst is proposed in Fig. 5. In this scheme, adsorption of OH^- species via one electron
28 transfer is the first step, and then followed by the formation of O–O bond in the OOH group. The
29 terminal step involves the disproportionation of higher valent oxide (CoO_2) to lower valent oxide
30 (CoO), and thus releasing oxygen.
31
32

33
34 From the results of our work and the literature, isotope labeling experiments together with mass
35 spectrometry studies have revealed that a lattice oxygen exchange mechanism is dependent on
36 structure, composition, metal-oxygen covalency and crystallinity of the catalyst.^{18,23,27,32} For
37 example, Shao-Horn et al. showed the lack of oxygen exchange on polycrystalline film and
38 nanocrystalline particles RuO_2 in contrast to the results of Wohlfahrt-Mehrens and Krtil and their
39 coworkers who demonstrated the involvement of lattice oxygen during OER. This discrepancy
40 might be due to the different surface crystallinity or the presence of defect active sites that are
41 formed during the different synthesis procedures of polycrystalline RuO_2 .^{18,23} Another parameter
42 that influences the involvement of lattice oxygen in OER is the metal-oxygen covalency as
43
44
45
46
47
48
49
50
51
52
53
54
55
56
57
58
59
60

demonstrated for perovskites by Shao-Horn et al.³² This difference in behavior emphasizes the critical role of the preparation conditions on the mechanism.

Further application of the isotope labeling procedure to other catalysts and systematic investigation of the effect of potential window could be valuable for mechanistic investigations. Moreover, the new cell design, first, allows the use of small volume of electrolyte, second, offers the use of particle layers and in particular those which are not stable enough for working under flow-through conditions, and third, provides a very short delay time. The exploitation of these features could add new opportunities for future studies: characterization of submonolayer amounts of organic adsorbates on electrode surfaces because of its high sensitivity; batteries and fuel cells research as well as evaluation of enzyme activities.

Table 2. Summary of results of estimation of true surface area of different catalysts and loadings using different methods.

Method Catalyst		Ball model	BET	DL-cap. method	Isotope exchange exp. A	Surface atoms exchanged (per BET area)	Redox peak method	Isotope exchange exp. B [#]
Co ₃ O ₄ (40μm) 100 μg/cm ² in 0.5M KOH with 2% isotope till 1.62V ²²	A_{tr} (cm ² _{tr} /cm ² _{geo})	0.016	--	12	0.72	--	2.1	0.28
	n (nmol/cm ² _{geo})	0.03	--	22	1.34		3.9	0.51
Co ₃ O ₄ (50nm) 200 μg/cm ² in 0.1M LiOH with 10% isotope till 1.8V ²²	A_{tr} (cm ² _{tr} /cm ² _{geo})	39	33	140	3.9	12%	32	1.8
	n (nmol/cm ² _{geo})	72	61	255	7.3		59	3.4
Co ₃ O ₄ (50 nm) 400 μg/cm ² in 0.8 M LiOH with 20% isotope till 1.6V	A_{tr} (cm ² _{tr} /cm ² _{geo})	79	66	68	7.3	12%	29	1.8
	n (nmol/cm ² _{geo})	145	122	126	13.5		53	3.4
Co ₃ O ₄ (50 nm) 400 μg/cm ² in 0.5 M LiOH with 50% isotope till 1.65 V (1.60 V) [*]	A_{tr} (cm ² _{tr} /cm ² _{geo})	79	66	105(89)	5.2(8)	8(13)%	23(22)	2.4(0.7)
	n (nmol/cm ² _{geo})	145	122	194(165)	9.7(15)		42(41)	4.5(1.3)
Co ₃ O ₄ (10 μm) 600 μg/cm ² in 0.8 M LiOH with 20% isotope till 1.61 V	A_{tr} (cm ² _{tr} /cm ² _{geo})	0.6	14	25	3.4	24%	--	1.3
	n (nmol/cm ² _{geo})	1.0	25	45	6.2		--	2.4
£Ag+Co ₃ O ₄ (50 nm) 10 w%, 400 μg/cm ² in 0.5 M LiOH with 50% isotope till 1.65 V	A_{tr} (cm ² _{tr} /cm ² _{geo})	8	6.6	77	3.2	50%	--	0.9
	n (nmol/cm ² _{geo})	15	12	142	5.9		--	1.6
£Ag+Co ₃ O ₄ (50 nm) 10 w%, 600 μg/cm ² in 0.8M LiOH with 20% isotope till 1.65 V	A_{tr} (cm ² _{tr} /cm ² _{geo})	12	9.9	44	3.8	40%	--	0.1
	n (nmol/cm ² _{geo})	22	18	81	7.1		--	0.2

[#] Isotope exchange in H₂¹⁸O-free solution after Co₃O₄ labeling (i.e. in series B)

£ Calculations were done with respect to only the mass of Co₃O₄ (50 nm) in the mixture.

* Repeated experiments with different upper potential limit.

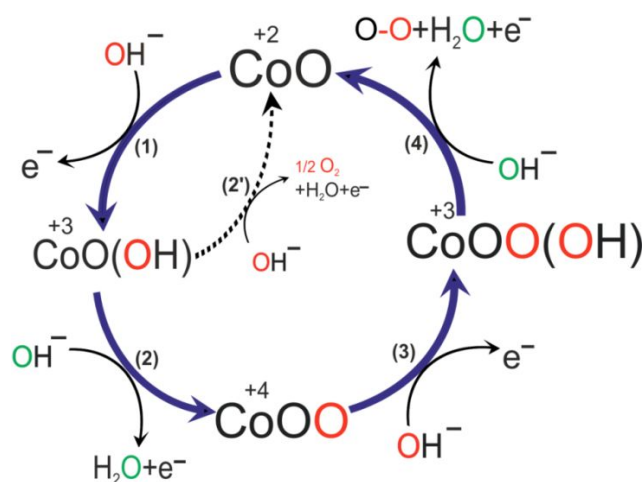


Fig. 5. Proposed scheme for oxygen evolution reaction on cobalt-containing spinel catalyst in alkaline media. After one OER cycle, some of O-atoms in the oxide, Co^{2+}O , will be exchanged with ^{18}O atoms (red).

5. Conclusions

In this study, we extend our investigations of oxygen exchange process to different particle sizes of Co_3O_4 as well as to the mixed $\text{Ag}+\text{Co}_3\text{O}_4$ catalyst. For the first time, we present a new *small-volume* DEMS cell design, which allows measurements on nanoparticle-modified disc electrodes and uses only sub-milliliters of electrolyte during measurement. The feasibility of the new cell is achieved by monitoring OER reaction. This cell shows a good performance and a very short delay time (1–2 s). We found that in H_2^{18}O -marked solution, the concentration of $^{16}\text{O}^{18}\text{O}$ increases in parallel to a decrease in $^{16}\text{O}_2$ concentration with each cycle before reaching a steady-state value. Thus suggests that the oxide takes part in OER. Only the outermost parts of the catalyst are active: $\sim 0.2\%$ of the total loading. Interestingly, the amount of oxygen exchanged on the mixed $\text{Ag} + \text{Co}_3\text{O}_4$ catalyst is higher than that at the single Co_3O_4 , which can be a possible origin of the improved electrocatalytic activity previously observed on the mixed catalyst. The real surface area of the catalysts is estimated using different methods and the results are compared. The electroanalytical approach presented here can lead to more in-depth studies that promote advances in electrocatalysis and electroanalysis.

Supporting Information

Experimental details; RRDE measurements; Additional isotope exchange results on Co_3O_4 (50 nm), Co_3O_4 (10 μm) and the mixed $\text{Ag}+\text{Co}_3\text{O}_4$; SEM of the mixed catalyst.

Acknowledgements

This work was supported by the Federal Ministry of Education and Research of Germany (BMBF) through the project "Strom aus Luft und Li" (03X4624A). H.M. Amin acknowledges the financial support from MoHE (Egypt) and DAAD. The authors thank S. K. Eswara and U. Kaiser for performing SEM and D. Wittmaier and K. A. Friedrich for providing the BET data.

6. References

- (1) McCrory, C. C. L.; Jung, S.; Ferrer, I. M.; Chatman, S. M.; Peters, J. C.; Jaramillo, T. F. *J. Am. Chem. Soc.* **2015**, *137*, 4347-4357.
- (2) Trotochaud, L.; Young, S. L.; Ranney, J. K.; Boettcher, S. W. *J. Am. Chem. Soc.* **2014**, *136*, 6744-6753.
- (3) Reier, T.; Oezaslan, M.; Strasser, P. *ACS Catal.* **2012**, *2*, 1765-1772.
- (4) Amin, H.; J. Bondue, C.; Eswara, S.; Kaiser, U.; Baltruschat, H. *Electrocatalysis* **2017**, *8*, 540-553.
- (5) Eßmann, V.; Barwe, S.; Masa, J.; Schuhmann, W. *Anal. Chem.* **2016**, *88*, 8835-8840.
- (6) Koza, J. A.; He, Z.; Miller, A. S.; Switzer, J. A. *Chem. Mater.* **2012**, *24*, 3567-3573.
- (7) Lee, Y.; Suntivich, J.; May, K. J.; Perry, E. E.; Shao-Horn, Y. *The Journal of Physical Chemistry Letters* **2012**, *3*, 399-404.
- (8) Trasatti, S. *J. Electroanal. Chem.* **1980**, *111*, 125-131.
- (9) Bockris, J. O. M.; Otagawa, T. *J. Electrochem. Soc.* **1984**, *131*, 290-302.
- (10) Hoang, T. T. H.; Gewirth, A. A. *ACS Catalysis* **2016**, *6*, 1159-1164.
- (11) Amin, H. M. A.; Baltruschat, H.; Wittmaier, D.; Friedrich, K. A. *Electrochim. Acta* **2015**, *151*, 332-339.
- (12) Wittmaier, D.; Wagner, N.; Friedrich, K. A.; Amin, H. M. A.; Baltruschat, H. *Journal of Power Sources* **2014**, *265*, 299-308.
- (13) Jiang, Z. Q.; Jiang, Z. J.; Maiyalagan, T.; Manthiram, A. *J. Mater. Chem. A* **2016**, *4*, 5877.
- (14) Rossmeisl, J.; Qu, Z. W.; Zhu, H.; Kroes, G. J.; Nørskov, J. K. *Journal of Electroanalytical Chemistry* **2007**, *607*, 83-89.
- (15) Suntivich, J.; May, K. J.; Gasteiger, H. A.; Goodenough, J. B.; Shao-Horn, Y. *Science* **2011**, *334*, 1383-1385.
- (16) Plaisance, C. P.; van Santen, R. A. *J. Am. Chem. Soc.* **2015**, *137*, 14660-14672.
- (17) Hamdani, M.; Singh, R. N.; Chartier, P. *International Journal of Electrochemical Science* **2010**, *5*, 556-577.
- (18) Stoerzinger, K. A.; Diaz-Morales, O.; Kolb, M.; Rao, R. R.; Frydendal, R.; Qiao, L.; Wang, X. R.; Halck, N. B.; Rossmeisl, J.; Hansen, H. A.; Vegge, T.; Stephens, I. E. L.; Koper, M. T. M.; Shao-Horn, Y. *ACS Energy Letters* **2017**, *2*, 876-881.
- (19) Wittmaier, D.; Cañas, N. A.; Biswas, I.; Friedrich, K. A. *Advanced Energy Materials* **2015**, *5*, 1500763.
- (20) Bergmann, A.; Martinez-Moreno, E.; Teschner, D.; Chernev, P.; Gliech, M.; de Araújo, J. F.; Reier, T.; Dau, H.; Strasser, P. *Nature Communications* **2015**, *6*, 8625.
- (21) Liu, Y.-C.; Koza, J. A.; Switzer, J. A. *Electrochim. Acta* **2014**, *140*, 359-365.
- (22) Amin, H. M. A.; Baltruschat, H. *Phys. Chem. Chem. Phys.* **2017**, *19*, 25527-25536.
- (23) Wohlfahrt-Mehrens, M.; Heitbaum, J. *J. Electroanal. Chem. Interfacial Electrochem.* **1987**, *237*, 251-260.
- (24) Fierro, S.; Nagel, T.; Baltruschat, H.; Comninellis, C. *Electrochem. Commun.* **2007**, *9*, 1969-1974.
- (25) Fierro, S.; Nagel, T.; Baltruschat, H.; Comninellis, C. *Electrochem. Solid State Lett.* **2008**, *11*, E20-E23.
- (26) Fierro, S.; Ouattara, L.; Calderon, E. H.; Passas-Lagos, E.; Baltruschat, H.; Comninellis, C. *Electrochim. Acta* **2009**, *54*, 2053-2061.
- (27) Roy, C.; Sebok, B.; Scott, S. B.; Fiordaliso, E. M.; Sørensen, J. E.; Bodin, A.; Trimarco, D. B.; Damsgaard, C. D.; Vesborg, P. C. K.; Hansen, O.; Stephens, I. E. L.; Kibsgaard, J.; Chorkendorff, I. *Nature Catalysis* **2018**, *1*, 820-829.
- (28) Jirkovský, J.; Makarova, M.; Krtil, P. *Electrochem. Commun.* **2006**, *8*, 1417-1422.
- (29) Wohlfahrt-Mehrens, M.; Heitbaum, J. *Journal of Electroanalytical Chemistry* **1987**, *237*, 251-260.
- (30) Macounova, K.; Makarova, M.; Krtil, P. *Electrochemistry Communications* **2009**, *11*, 1865-1868.
- (31) Fabbri, E.; Nachttegaal, M.; Binninger, T.; Cheng, X.; Kim, B.-J.; Durst, J.; Bozza, F.; Graule, T.; Schäublin, R.; Wiles, L.; Pertoso, M.; Danilovic, N.; Ayers, K. E.; Schmidt, T. *Nature Materials* **2017**, *16*, 925.
- (32) Grimaud, A.; Diaz-Morales, O.; Han, B.; Hong, W. T.; Lee, Y.-L.; Giordano, L.; Stoerzinger, K. A.; Koper, M. T. M.; Shao-Horn, Y. *Nature Chemistry* **2017**, *9*, 457.
- (33) Baltruschat, H. *Journal of the American Society for Mass Spectrometry* **2004**, *15*, 1693-1706.
- (34) Trimarco, D. B.; Pedersen, T.; Hansen, O.; Chorkendorff, I.; Vesborg, P. C. K. *Review of Scientific Instruments* **2015**, *86*, 075006.
- (35) Wang, H.; Rus, E.; Sakuraba, T.; Kikuchi, J.; Kiya, Y.; Abruña, H. D. *Anal. Chem.* **2014**, *86*, 6197-6201.
- (36) Hartung, T.; Baltruschat, H. *Langmuir* **1990**, *6*, 953-957.
- (37) Heinen, M.; Chen, Y. X.; Jusys, Z.; Behm, R. J. *Electrochim. Acta* **2007**, *52*, 5634-5643.
- (38) Bawol, P. P.; Reinsberg, P. H.; Baltruschat, H. *Anal. Chem.* **2018**, *90*, 14145-14149.

1
2 (39) Bani Hashemi, A.; La Mantia, F. *Anal. Chem.* **2016**, *88*, 7916-7920.

3 (40) Trimarco, D. B.; Scott, S. B.; Thilsted, A. H.; Pan, J. Y.; Pedersen, T.; Hansen, O.; Chorkendorff, I.; Vesborg, P. C. K. *Electrochim. Acta* **2018**,
4 *268*, 520-530.

5 (41) Levine, S.; Smith, A. L. *Discussions of the Faraday Society* **1971**, *52*, 290-301.
6
7

8
9 **TOC:**
10

